

# Orbital-Selective Spin-Triplet Superconductivity in Infinite-Layer Lanthanum Nickelates

Fabian Jakubczyk,<sup>1,2,\*</sup> Armando Consiglio,<sup>3,2</sup> Domenico Di Sante,<sup>4</sup> Ronny Thomale,<sup>3,2</sup> and Carsten Timm<sup>1,2</sup>

<sup>1</sup>*Institute of Theoretical Physics, Technische Universität Dresden, 01069 Dresden, Germany*

<sup>2</sup>*Würzburg-Dresden Cluster of Excellence ct.qmat, Germany*

<sup>3</sup>*Institut für Theoretische Physik und Astrophysik,*

*Universität Würzburg, 97074 Würzburg, Germany*

<sup>4</sup>*Department of Physics and Astronomy, University of Bologna, 40127 Bologna, Italy*

(Dated: March 29, 2024)

The discovery of superconductivity in infinite-layer nickelates has ignited stark interest within the scientific community, particularly regarding its likely unconventional origin. Conflicting magnetotransport measurements report either isotropic or anisotropic suppression of superconductivity in an external magnetic field, with distinct implications for the nature of superconducting order. In order to ensure a most suited model subject to subsequent many-body analysis, we develop a first-principles-guided minimal theory including Ni  $d_{x^2-y^2}$ , La  $d_{3z^2-r^2}$ , and La  $d_{xy}$  orbitals. Amended by the consideration of orbital-selective pairing formation, which emphasises the correlation state of the Ni  $3d_{x^2-y^2}$  orbital, we calculate the superconducting ordering susceptibility mediated by spin fluctuations. We find a parametric competition between even-parity  $d$ -wave and, in contrast to previous studies, odd-parity  $p$ -wave pairing, which becomes favorable through a large quasiparticle weight renormalization for Ni  $3d_{x^2-y^2}$  electrons. Our findings not only shed light on the distinctiveness of LaNiO<sub>2</sub> as compared to cuprate superconductors or nickelates of different rare-earth composition but also provoke similarities to other pending candidate odd-parity superconductors.

*Introduction.*—Since the initial discovery of superconductivity in Sr-doped NdNiO<sub>2</sub> thin films [1], the family of nickelate superconductors has kept on growing and by now also includes La<sub>1-x</sub>Sr<sub>x</sub>NiO<sub>2</sub>, Pr<sub>1-x</sub>Sr<sub>x</sub>NiO<sub>2</sub>, and La<sub>1-x</sub>Ca<sub>x</sub>NiO<sub>2</sub> [2, 3]. Most intriguingly, some groups report the onset of superconductivity even in undoped LaNiO<sub>2</sub>, suggesting that the eventual ground state of sufficiently clean undoped infinite-layer (IL) nickelates may be a superconducting (SC) state [2, 4, 5]. Despite being isostructural to high  $T_c$  cuprates, the extend of similarity between these materials remains partially unclear, in spite of numerous studies addressing this issue [6–10].

For instance, parent cuprates exhibit long-range antiferromagnetic order, whereas clear signatures of long-range magnetism are lacking in bulk LaNiO<sub>2</sub> and NdNiO<sub>2</sub> [11–13]. Nevertheless, cuprate-like magnetic excitations have been observed in NdNiO<sub>2</sub> films using resonant inelastic x-ray scattering [14]. Recent measurements applying a superconducting quantum interference device (SQUID) reported a relatively uniform paramagnetic response in La<sub>0.85</sub>Sr<sub>0.15</sub>NiO<sub>2</sub>, together with an inhomogeneous ferromagnetic background independent of the specific rare-earth (RE) ion [15]. Moreover, a short-range ordered ground state was observed by muon spin rotation measurements [4]. Magnetism is often triggered by strong electronic correlations, which indeed are present in IL nickelates [7, 16–18]. However, the coupling to itinerant RE electrons might lead to the suppression of magnetism [7, 14]. Similar to the question of magnetic instabilities in IL nickelates, the symmetry of the SC order-parameter (OP) remains unsettled. On the one hand, magnetotransport measurements indicate isotropic Pauli-limited

behavior with singlet pairing and even parity in the IL nickelate Nd<sub>0.775</sub>Sr<sub>0.225</sub>NiO<sub>2</sub> [19]. This scenario was supported by many theoretical investigations, mostly pointing at  $d$ -wave order like in the cuprates [16, 20–24]. On the other hand, evidence for anisotropic superconductivity that violates Pauli limiting and potential spin-triplet pairing was reported in La-based nickelate thin films [5, 25, 26]. Likewise, this anisotropic limiting behavior for different magnetic-field orientations has recently been observed for free-standing IL nickelate membranes [27]. Variations in the upper critical field within the nickelate family were ascribed to the different RE elements, i.e., the magnetic character of the  $4f$  electrons for the Nd<sup>3+</sup> Kramers doublet as opposed to their absence in La<sup>3+</sup>, or the nonmagnetic singlet ground state of Pr<sup>3+</sup> [28].

In this Letter, we address the open question of gap structure and potential odd-parity pairing in IL LaNiO<sub>2</sub>. So far, LaNiO<sub>2</sub> appears to be the only member of the nickelate family showing signatures of superconductivity in the absence of doping. This places it in a regime where the largest deviation from the cuprates as well as the strongest effective-mass enhancement can be expected. A direct comparison between for instance NdNiO<sub>2</sub> and LaNiO<sub>2</sub> reveals that this effect is particularly strong in the lanthanum compound [16]. Moreover, LaNiO<sub>2</sub> does not host any  $4f$  electrons, who may influence the SC pairing [29]. Hybridization with  $4f$  electrons is expected to be non-negligible in Nd and Pr nickelates [29–32]. To resolve this puzzle, we adopt the perspective of spin-fluctuation-mediated unconventional superconductivity [33] and incorporate the effect of increased correlations via the orbital-selective approach known from iron-based super-

conductors [34, 35]. Our calculations reveal that spin-triplet pairing can indeed be realized in  $\text{LaNiO}_2$ , once an enhanced effective mass of the  $\text{Ni } 3d_{x^2-y^2}$  electrons is taken into account.

*Low-energy electronic structure.*—In non-magnetic  $\text{LaNiO}_2$ , the principal contribution at the Fermi level arises from a band primarily governed by  $\text{Ni } 3d_{x^2-y^2}$  electrons. This results in a large hole-like and mostly two-dimensional (2D) Fermi surface (FS) similar to the cuprates. In addition, another hybridized band of mixed  $\text{Ni } 3d$  and  $\text{La } 5d$  character creates small ellipsoidal, electron-like pockets around the  $\Gamma$  and A high-symmetry points of the Brillouin zone, indicating the multi-orbital and three-dimensional (3D) character of  $\text{LaNiO}_2$  [10, 36, 37]. These two electron pockets enable self-hole-doping of the large  $d_{x^2-y^2}$  Fermi sheet, a process with major involvement of  $\text{La } 5d$  states [7, 17]. Especially  $\text{La } 5d_{z^2}$  and  $\text{La } 5d_{xy}$  orbitals are known to have significant weight on the FS [7, 10, 20], where  $d_{z^2}$  is a shorthand notation for  $d_{3z^2-r^2}$ . Furthermore, these partially occupied electron pockets might give rise to the negative Hall coefficient, to the slightly metallic behavior of the resistivity at high temperatures, and possibly even to the superconductivity in undoped IL nickelates [2, 3, 20].

Hole-doping the system for instance with Sr induces changes in the electronic structure. It reduces the self-doping effect by first shifting the  $\Gamma$  pocket above  $E_F$ , followed by the pocket around A in the overdoped region [7, 16, 38–40]. Furthermore, doping reduces the charge-transfer energy [38], i.e., overall increases the cuprate-like character of the nickelates. However, the impact on  $\text{LaNiO}_2$  is expected to be less pronounced compared to Nd-/Pr-based compounds regarding charge carriers, which is evidenced by the persistent negative Hall coefficient of  $\text{La}_{1-x}\text{Sr}_x\text{NiO}_2$  even upon doping [2, 3].

In our effective low-energy Hamiltonian we thus include  $\text{Ni } d_{x^2-y^2}$ ,  $\text{La } d_{z^2}$ , and  $\text{La } d_{xy}$  orbitals and introduce the operator  $\psi_\sigma^\dagger(\mathbf{k}) = [c_{1\sigma}^\dagger(\mathbf{k}), c_{2\sigma}^\dagger(\mathbf{k}), c_{3\sigma}^\dagger(\mathbf{k})]$  to describe the given multiband system. Here,  $c_{l\sigma}^\dagger(\mathbf{k})$  is the fermionic creation operator, where  $\sigma$  and  $l$  denote the spin and orbital index, with  $l = 1, 2, 3$  referring to the  $\text{La } 5d_{z^2}$ ,  $\text{La } 5d_{xy}$ , and  $\text{Ni } 3d_{x^2-y^2}$  orbital, respectively. We thus write the non-interacting Hamiltonian as

$$H_0 = \sum_{\mathbf{k}\sigma} \psi_\sigma^\dagger(\mathbf{k}) h(\mathbf{k}) \psi_\sigma(\mathbf{k}), \quad (1)$$

where  $h(\mathbf{k})$  is constructed utilizing hopping amplitudes obtained from the Wannier downfolding of the band structure derived from density functional theory (DFT). Thereby, we capture the important characteristics, as well as the distribution of orbital characters, of the non-magnetic FS in agreement with previous DFT [20, 30, 41] and alternative approaches such as DFT+ $U$  [7, 42], DFT + dynamical mean-field theory (DMFT) [18, 36] or the  $GW$  approximation [43]. Details on the ab-initio calculations as well as the Hamiltonian  $h(\mathbf{k})$  are given in the

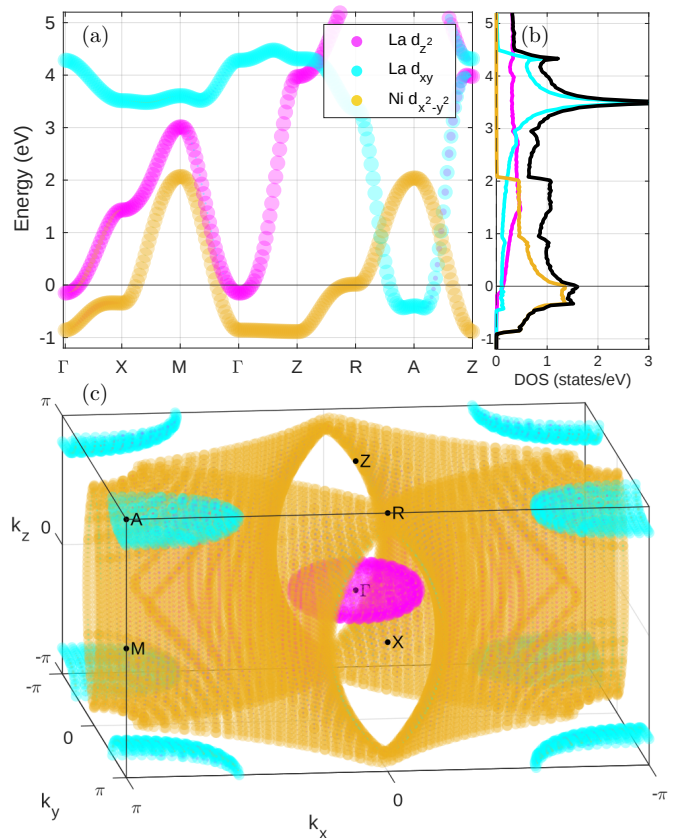


FIG. 1. (a) Band structure, (b) density of states, and (c) 3D Fermi surface including the orbital contributions relevant for the low-energy description of pristin  $\text{LaNiO}_2$ . Magenta, cyan, and yellow refer to the  $\text{La } d_{z^2}$ ,  $\text{La } d_{xy}$ , and  $\text{Ni } d_{x^2-y^2}$  orbitals, respectively.

Supplemental Material (SM) [44]. In Fig. 1, we plot the orbitally resolved single-particle band structure, as well as the corresponding 3D FS and density of states (DOS) of our minimal model. Here,  $\text{La } 5d_{z^2}$  weight is located mostly around  $\Gamma$ , while the  $\text{La } 5d_{xy}$  electrons have a major contribution around the A point.

*Strong correlations and magnetic response.*—Orbitally differentiated correlations play an important role in IL nickelates. In particular the  $\text{Ni } 3d_{x^2-y^2}$  electrons are highly correlated, suggesting that they are in the vicinity of a Mott critical regime [36]. This is evidenced by an enhanced effective mass and thus reduced quasiparticle weight  $Z$ , which is significantly smaller for the  $\text{Ni } d_{x^2-y^2}$  orbital compared to the other  $3d$  orbitals [16, 18, 23]. In our work, we therefore focus on the effect of a highly correlated  $\text{Ni } d_{x^2-y^2}$  orbital. Previous studies have reported specific values of either the effective mass or the renormalization factor ( $m^*/m = 1/Z$ ) in  $\text{LaNiO}_2$ , ranging from  $m^*/m \approx 2.81$  ( $Z_{d_{x^2-y^2}} \approx 0.35$ ) [18, 36], over  $m^*/m \approx 4.1$  ( $Z_{d_{x^2-y^2}} \approx 0.24$ ) [45] to  $m^*/m \approx 5.5$  ( $Z_{d_{x^2-y^2}} \approx 0.18$ ) [16] or even lower ( $Z_{d_{x^2-y^2}} \approx 0$ ) [23]. These values specify a reasonable range of  $Z_{d_{x^2-y^2}}$ . More-

over, doping would shift the Ni  $d_{x^2-y^2}$  orbital away from half-filling, where electronic correlations are strongest. Therefore, a decrease of the mass enhancement with doping was reported [16, 23, 36, 45].

We take this correlation-induced renormalization into account by means of the orbital selective ansatz [34, 35]. In this ansatz, quasiparticles in orbital  $l$  are weighted by a factor  $\sqrt{Z_l}$ , i.e.,  $c_l^\dagger(\mathbf{k}) \rightarrow \sqrt{Z_l}c_l^\dagger(\mathbf{k})$  and the Green's function in the orbital basis becomes

$$\tilde{G}_{ll'}(\mathbf{k}, \omega_n) = \sqrt{Z_l Z_{l'}} \sum_{\mu} \frac{a_{\mu}^l(\mathbf{k}) a_{\mu}^{l'*}(\mathbf{k})}{i\omega_n - E_{\mu}(\mathbf{k})}, \quad (2)$$

where  $E_{\mu}(\mathbf{k})$  is the eigenenergy of band  $\mu$ . Subsequently, the bare susceptibility in orbital space  $\chi_{l_1 l_2 l_3 l_4}^0$  requires a straightforward multiplication by the quasiparticle weights to derive the corresponding quantity

$$\tilde{\chi}_{l_1 l_2 l_3 l_4}^0(\mathbf{q}, \omega) = \sqrt{Z_{l_1} Z_{l_2} Z_{l_3} Z_{l_4}} \chi_{l_1 l_2 l_3 l_4}^0(\mathbf{q}, \omega) \quad (3)$$

in the correlated system [34, 35, 46].

In the next step, we introduce local electron-electron interactions via a multiorbital Hubbard-Hund Hamiltonian

$$\begin{aligned} H_{\text{int}} = & U_{\text{Ni}} \sum_i n_{i\uparrow} n_{i\downarrow} \\ & + U_{\text{La}} \sum_i n_{i\uparrow} n_{i\downarrow} + U'_{\text{La}} \sum_{i,l,l'} n_{il} n_{il'} \\ & + J_{\text{La}} \sum_{i,l,l'} \sum_{\sigma,\sigma'} c_{i\uparrow\sigma}^\dagger c_{i'l'\sigma'}^\dagger c_{i\downarrow\sigma} c_{i'l'\sigma} \\ & + J'_{\text{La}} \sum_{i,l,l'} c_{i\uparrow}^\dagger c_{i\downarrow}^\dagger c_{i'l'} c_{i'l'\uparrow}, \end{aligned} \quad (4)$$

where the coupling constants  $U$ ,  $U'$ ,  $J$ , and  $J'$  denote the intraorbital Coulomb, interorbital Coulomb, Hund's, and pair-hopping interactions, respectively. The orbital indices  $l, l' \in (1, 2)$  run over the La  $5d$  orbitals  $d_{z^2}$  and  $d_{xy}$  since for Ni only on-site Coulomb repulsion is considered. Throughout our calculations, we apply the relations  $U' = U - (J + J')$  and  $J' = J$  between the coupling constants, which are satisfied in various orbital degenerate models and if orbital wave functions can be chosen real [47, 48]. Furthermore, we choose reference values from literature to get a reasonable estimate of interaction strengths in this material, namely  $U_{\text{La}}/U_{\text{Ni}} \approx 0.5$  and  $J_{\text{La}}/U_{\text{La}} \approx 0.2$  [18, 20, 23, 36, 49]. Especially the inclusion of on-site Hund's coupling  $J$ , i.e., of intra-atomic exchange interactions is expected to be a vital ingredient for capturing the correlation physics. LaNiO<sub>2</sub> shows characteristic Hund's metal signatures such as the unexpected absence of magnetism, the importance of high-spin configurations, metallicities, orbital differentiation, and a decrease of  $Z_{d_{x^2-y^2}}$  with stronger Hund's coupling  $J$  [18, 23, 36, 49]. These interactions are included in the calculation of susceptibilities within the random phase

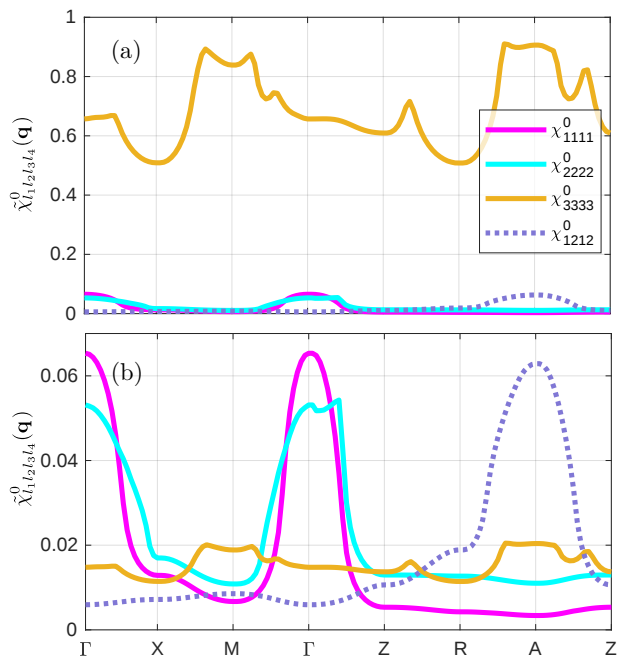


FIG. 2. Static bare susceptibilities  $\tilde{\chi}_{l_1 l_2 l_3 l_4}^0(\mathbf{q}, \omega = 0)$  of parent LaNiO<sub>2</sub> for (a)  $Z_{d_{x^2-y^2}} = 1$  and (b)  $Z_{d_{x^2-y^2}} = 0.15$ . Magenta, cyan, and yellow refer to the pure La  $d_{z^2}$ , La  $d_{xy}$  and Ni  $d_{x^2-y^2}$  orbital contributions, respectively. The off-diagonal  $\tilde{\chi}_{1212}^0$  bare susceptibility is shown in purple. We use  $80 \times 80 \times 80$   $\mathbf{k}$ -points for momentum space integration.

approximation (RPA). Note that in RPA the spin susceptibility systematically diverges once the interaction exceeds a critical value  $U_c$  and indicates a spin-density-wave instability, below which superconductivity emerges induced by spin fluctuations. In the renormalized case, we set  $U_{\text{Ni}} = 5$  eV, while for  $Z_{d_{x^2-y^2}} = 1$  we use  $U_{\text{Ni}} = 0.5$  eV, since here  $U_c \approx 1$  eV. Note that  $U_c$  is a phenomenological parameter, which does not facilitate an immediate quantitative linkage with the bare interaction strength.

In Figs. 2(a) and 2(b), the non-interacting susceptibilities  $\tilde{\chi}_{l_1 l_2 l_3 l_4}^0(\mathbf{q}, 0)$  are shown separately for the orbital contributions  $l = 1, 2, 3$  referring to La  $5d_{z^2}$ , La  $5d_{xy}$ , and Ni  $3d_{x^2-y^2}$ , respectively. Figure 2(a) addresses the unrenormalized case, with the main peaks located around the M and A points, similar to the cuprates [50]. These magnetic fluctuations are dominated by Ni  $d_{x^2-y^2}$  electrons and strongly enhanced upon introducing interactions at the RPA level. In contrast, the diagonal contributions of the La  $d_{z^2}$  and  $d_{xy}$  orbital reach their maximum around  $\Gamma$ . Moreover, we observe a sizeable off-diagonal  $\tilde{\chi}_{1212}^0$  feature around the A point, keeping in mind that  $\tilde{\chi}_{abcd}^0 = \tilde{\chi}_{dcba}^0$  for inversion-symmetric systems.

Sufficient reduction of the Ni  $d_{x^2-y^2}$  quasiparticle weight eventually leads to a clear dominance of fluctuations stemming from the RE orbitals, as can be seen in Fig. 2(b), where  $Z_{d_{x^2-y^2}} = 0.15$ . Therefore, fluctuations are becoming more three dimensional, reflecting the 3D

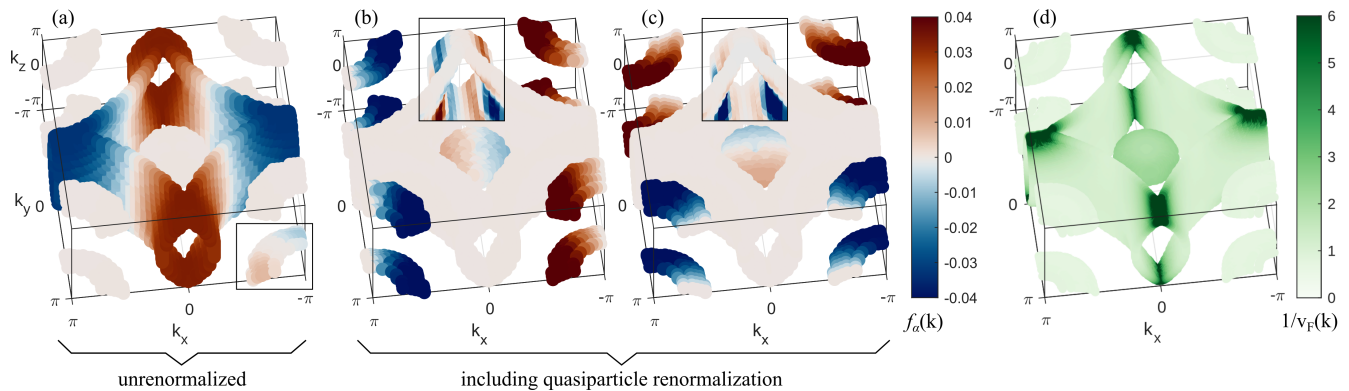


FIG. 3. Leading pairing structure of LaNiO<sub>2</sub> (b), (c) with and (a) without inclusion of quasiparticle renormalization. The gap symmetry changes from (a) an even-parity *d*-wave to (b), (c) a degenerate odd-parity *p*-wave solution. A colorscale highlighting smaller amplitudes with maximum value of  $\pm 1 \times 10^{-4}$  was chosen for the insets to reveal, e.g., in panels (b), (c), the horizontal line nodes on the large FS for  $k_z = \pm\pi/2$ . (d) Inverse Fermi-velocity  $1/v_F(\mathbf{k}) = 1/|\nabla_{\mathbf{k}}E_{\nu}(\mathbf{k})|$  giving a measure of the DOS.

character of LaNiO<sub>2</sub>. Interactions predominantly lead to an enhancement of the diagonal La *5d* peaks around  $\Gamma$  but also of mixed orbital  $\tilde{\chi}_{1122}^{\text{RPA},s}$  and  $\tilde{\chi}_{1221}^{\text{RPA},s}$  contributions around  $\Gamma$  and A, respectively. The latter are not notable on the bare level but in particular the  $\tilde{\chi}_{1122}^{\text{RPA},s}$  component diverges together with the intra-orbital spin susceptibilities  $\tilde{\chi}_{1111}^{\text{RPA},s}$  and  $\tilde{\chi}_{2222}^{\text{RPA},s}$  upon approaching  $U_c$ . Previous calculations of the LaNiO<sub>2</sub> static weak-coupling spin susceptibility for  $\mathbf{q} = (q_x, q_y, 0)$  with converged DFT + DMFT Green's functions including self-interaction corrections similarly resulted in a maximum near  $\Gamma$  [17]. Such a transition stresses the necessity of reevaluating the SC pairing symmetries in the regime of strongly renormalized Ni *3d* quasiparticle weights.

*Spin-fluctuation pairing.*— Magnetic fluctuations are seen as a strong candidate for mediating superconductivity in IL nickelates [12–14, 16, 20, 21, 30, 46, 51]. In order to compute the SC pairing interactions, we thus employ a formalism based on spin-fluctuations [52–54] with the adjustment of additional quasiparticle renormalization when projecting the pairing interaction from orbital to band space [35, 46]. For this purpose, we solve the linearized gap equation

$$\lambda_{\alpha} f_{\alpha}(\mathbf{k}) = \sum_j \oint_{C_j} \frac{d^2 k'_{\parallel}}{(2\pi)^2 v_F(\mathbf{k}')} \tilde{\Gamma}_{ij}(\mathbf{k}, \mathbf{k}') f_{\alpha}(\mathbf{k}'), \quad (5)$$

the eigenvalues of which determine the pairing strength  $\lambda_{\alpha}$  for the various pairing channels  $\alpha$  [55]. The largest eigenvalue results in the highest transition temperature [53], while its eigenfunction  $f_{\alpha}(\mathbf{k})$  identifies the gap symmetry.  $\tilde{\Gamma}_{ij}(\mathbf{k}, \mathbf{k}')$  represents the renormalized form of the effective multiorbital pair scattering vertex and momenta  $\mathbf{k} \in C_i$ ,  $\mathbf{k}' \in C_j$  are constrained to the FS sheets  $C_{i,j}$ . A momentum-dependent measure of the DOS is given by the inverse Fermi velocity  $1/v_F(\mathbf{k}) = 1/|\nabla_{\mathbf{k}}E_{\nu}(\mathbf{k})|$ , which is shown in Fig. 3(d) for the rigid bands of our model. Here, van Hove features can be observed on the

hole-like FS near the R points. In order to convert the integral equation (5) to an algebraic matrix equation that can be solved numerically, the area of the discretized Fermi surface segments is determined using a Delaunay triangulation procedure [35, 56]. Within our calculations, we apply a mesh for momentum space integration with  $60 \times 60 \times 60$   $\mathbf{k}$ -points. A total of 8504 and 6800 points on all FS sheets is taken for 3D gap-structure calculations in pristine and doped LaNiO<sub>2</sub>, respectively.

In Fig. 3, we present the leading gap-symmetry functions  $f_{\alpha}(\mathbf{k})$  for (a) the unrenormalized and (b), (c) the renormalized scenario. Unsurprisingly, a simple *d*-wave singlet solution is clearly favored for  $Z_l = 1$ , i.e., when orbital-selective renormalization is disregarded. Such a state belongs to the  $B_{1g}$  irreducible representation of the point group  $D_{4h}$ , which describes the underlying tetragonal lattice. Here, Cooper pairing from the Ni  $3d_{x^2-y^2}$  orbital is predominant, with an almost vanishing gap on the RE electron pockets around  $\Gamma$  and A. This cuprate-like SC order has been suggested previously based on spin fluctuations [16, 20–22, 24, 46].

Once we shift our model into the strongly correlated regime of  $Z_{d_{x^2-y^2}} \lesssim 0.2$ , solving the linearized gap equation (5) yields drastically altered results. The SC gap is now largest on the La dominated pockets, since the Ni  $d_{x^2-y^2}$  quasiparticle DOS is strongly reduced. Moreover, the gap changes sign on the large FS as a function of  $k_z$ , leading to opposite signs on the pockets near  $\Gamma$  and A. Even more importantly, two degenerate *p*-wave solutions become favored. These belong to the two-dimensional representation  $E_u$  and are likely realized in the time-reversal-symmetry-breaking (TRSB) state, for which the weak-coupling condensation energy becomes largest compared to the remaining possible combinations of the  $p_x$  and  $p_y$  solution [57]. In the presence of weak spin-orbit coupling (see SM [44]), one naturally expects an alignment between the *z*-direction of the spin wave function

and the crystalline  $c$ -axis [58]. Therefore, we can analytically approximate the numerically calculated SC OP of this spin-triplet state by

$$\mathbf{d}(\mathbf{k}) = \Delta_0 \hat{\mathbf{z}} \cos k_z (\sin k_x \pm i \sin k_y), \quad (6)$$

with the magnitude of the quasiparticle gap

$$\Delta_{\mathbf{k}} = |\mathbf{d}(\mathbf{k})| = \Delta_0 \sqrt{\cos^2 k_z (\sin^2 k_x + \sin^2 k_y)}. \quad (7)$$

Such a state is often referred to as chiral  $p$ -wave. Moreover, it is analogous to the so-called Anderson-Brinkman-Morel (ABM or axial) phase of  $^3\text{He}$  [59, 60] and has been debated extensively, e.g., for  $\text{Sr}_2\text{RuO}_4$  [57, 58, 61]. The gap resulting from the  $\mathbf{d}$  vector in (6) has point nodes on the electron pockets for  $k_x, k_y = 0, \pm\pi$  and  $k_z = \pm k_F$ . In addition, line nodes are located on the large hole-like FS for  $k_x, k_y = k_F$  and  $k_z = \pm\pi/2$ . Besides, TRSB is accompanied by interesting magnetic properties, since the OP in Eq. (6) possesses orbital angular momentum  $m_z = \pm 1$  along the  $z$ -axis. Cooper pairs carry charge, hence the finite angular-momentum average over the FS induces a magnetic moment leading to a SC state with “ferromagnetic” properties. Intriguingly, our conclusions even hold when the effect of doping is included as a rigid shift of the chemical potential such that the pocket around  $\Gamma$  vanishes (see SM [44]). In fact, the transition to a favored  $p$ -wave happens for even bigger quasiparticle weights of  $Z_{d_{x^2-y^2}} \lesssim 0.3$ . However, a reduced mass enhancement due to doping might have a compensating effect. One potential yet unexplored scenario involves the doping-induced transition to a distinct OP within the SC dome.

Our proposal of chiral  $p$ -wave superconductivity with  $\mathbf{d} \parallel \hat{\mathbf{z}}$  could explain the experimentally observed weaker suppression of superconductivity for an external magnetic field oriented within the basal plane [5, 25, 27, 28]. For triplet superconductors, one would generally not expect Pauli suppression if  $\mathbf{d} \cdot \mathbf{H} = 0$ , i.e., the alignment  $\mathbf{d} \parallel \mathbf{H}$  maximizes paramagnetic limiting effects. Moreover, the gap in Eq. (7) has point nodes and thus could cause the quadratic temperature dependence of the London penetration depth [62, 63], which was attributed to a superconductor with line nodes in the presence of disorder [64, 65]. Small deviations from quadratic scaling may result from additional weight at the Fermi level, due to the horizontal line nodes on the Ni  $d_{x^2-y^2}$  dominated FS with low quasiparticle DOS. Besides, recent muon spin rotation measurements provided direct evidence for the coexistence of short-range magnetic order and superconductivity in IL nickelates [4], which indicates TRSB.

*Summary and conclusions.*— Our calculations of magnetic fluctuations and the resulting pairing symmetries reveal potential topological  $p_x + ip_y$  superconductivity in IL  $\text{LaNiO}_2$ , once an orbital-selective quasiparticle renormalization is introduced for the Ni  $d_{x^2-y^2}$  electrons. From our results, we can conclude that RE physics in  $\text{LaNiO}_2$  is not merely important for the explanation of

a negative Hall conductivity [2] but that superconductivity could actually emerge from the associated bands. However, one should keep in mind that the RE metal representative strongly affects the observed phenomenology of IL nickelates. Additionally, the proposed  $p$ -wave order would resolve the controversy surrounding the anisotropic high-field limiting behavior obtained from magnetotransport measurements [5, 25, 27], as well as the quadratic temperature dependence of the superfluid density [62, 63]. In this regard, our effective Hamiltonian captures the relevant physics for superconductivity in 112 lanthanum nickelates, highlighting the importance of multiorbital processes and the 3D fermiology. To conclude, our comprehensive investigation provides strong evidence that IL  $\text{LaNiO}_2$  could exhibit spin-triplet superconductivity, a phenomenon rarely observed. This result holds promise for a new research direction within the field of SC infinite-layer nickelates in particular and for the understanding of  $p$ -wave pairing in general.

We thank Brian M. Andersen, Astrid T. Rømer, Ilya M. Eremin, Frank Lechermann, Berit H. Goodge, and Matteo Dürrnagel for useful discussions. Financial support by the Würzburg-Dresden Cluster of Excellence ct.qmat, EXC 2147, project ID 390858490 is gratefully acknowledged. C. Timm acknowledges funding by the Deutsche Forschungsgemeinschaft through Collaborative Research Center SFB 1143, project A04, project ID 247310070. R. Thomale and A. Consiglio acknowledge support through the SFB 1170 ToCoTronics, project ID 258499086. A. Consiglio, D. Di Sante and R. Thomale acknowledge the Gauss Centre for Supercomputing e.V. for providing computing time on the GCS Supercomputer SuperMUC at Leibniz Supercomputing Centre. D. Di Sante received funding from the European Union Horizon 2020 research and innovation program under the Marie Skłodowska-Curie Grant Agreement No. 897276. A. Consiglio acknowledges support from PNRR MUR project PE0000023-NQSTI.

---

\* fabian.jakubczyk@tu-dresden.de

- [1] D. Li, K. Lee, B. Y. Wang, M. Osada, S. Crossley, H. R. Lee, Y. Cui, Y. Hikita, and H. Y. Hwang, Superconductivity in an infinite-layer nickelate, *Nature* **572**, 624 (2019).
- [2] M. Osada, B. Y. Wang, B. H. Goodge, S. P. Harvey, K. Lee, D. Li, L. F. Kourkoutis, and H. Y. Hwang, Nickelate Superconductivity without Rare-Earth Magnetism:  $(\text{La},\text{Sr})\text{NiO}_2$ , *Adv. Mater.* **33**, 2104083 (2021).
- [3] S. Zeng, C. Li, L. E. Chow, Y. Cao, Z. Zhang, C. S. Tang, X. Yin, Z. S. Lim, J. Hu, P. Yang, and A. Ariando, Superconductivity in infinite-layer nickelate  $\text{La}_{1-x}\text{Ca}_x\text{NiO}_2$  thin films, *Sci. Adv.* **8**, eabl9927 (2022).
- [4] J. Fowlie, M. Hadjimichael, M. M. Martins, D. Li, M. Osada, B. Y. Wang, K. Lee, Y. Lee, Z. Salman, T. Prokscha,

- J.-M. Triscone, H. Y. Hwang, and A. Suter, Intrinsic magnetism in superconducting infinite-layer nickelates, *Nat. Phys.* **18**, 1043 (2022).
- [5] W. Sun, Y. Li, R. Liu, J. Yang, J. Li, W. Wei, G. Jin, S. Yan, H. Sun, W. Guo, Z. Gu, Z. Zhu, Y. Sun, Z. Shi, Y. Deng, X. Wang, and Y. Nie, Evidence for Anisotropic Superconductivity Beyond Pauli Limit in Infinite-Layer Lanthanum Nickelates, *Adv. Mater.* **35**, 2303400 (2023).
- [6] K.-W. Lee and W. E. Pickett, Infinite-layer  $\text{LaNiO}_2$ :  $\text{Ni}^{1+}$  is not  $\text{Cu}^{2+}$ , *Phys. Rev. B* **70**, 165109 (2004).
- [7] A. Botana and M. Norman, Similarities and Differences between  $\text{LaNiO}_2$  and  $\text{CaCuO}_2$  and Implications for Superconductivity, *Phys. Rev. X* **10**, 011024 (2020).
- [8] F. Lechermann, Late transition metal oxides with infinite-layer structure: Nickelates versus cuprates, *Phys. Rev. B* **101**, 081110 (2020).
- [9] V. I. Anisimov, D. Bukhvalov, and T. M. Rice, Electronic structure of possible nickelate analogs to the cuprates, *Phys. Rev. B* **59**, 7901 (1999).
- [10] M. Hepting, D. Li, C. J. Jia, H. Lu, E. Paris, Y. Tseng, X. Feng, M. Osada, E. Been, Y. Hikita, Y.-D. Chuang, Z. Hussain, K. J. Zhou, A. Nag, M. Garcia-Fernandez, M. Rossi, H. Y. Huang, D. J. Huang, Z. X. Shen, T. Schmitt, H. Y. Hwang, B. Moritz, J. Zaanen, T. P. Devereaux, and W. S. Lee, Electronic structure of the parent compound of superconducting infinite-layer nickelates, *Nat. Mater.* **19**, 381 (2020).
- [11] H. Lin, D. J. Gawryluk, Y. M. Klein, S. Huangfu, E. Pomjakushina, F. Von Rohr, and A. Schilling, Universal spin-glass behaviour in bulk  $\text{LaNiO}_2$ ,  $\text{PrNiO}_2$  and  $\text{NdNiO}_2$ , *New J. Phys.* **24**, 013022 (2022).
- [12] R. A. Ortiz, P. Pumphal, M. Klett, F. Hotz, R. K. Kremer, H. Trepka, M. Himmida, H.-A. K. Von Nidda, M. Isobe, R. Khasanov, H. Luetkens, P. Hansmann, B. Keimer, T. Schäfer, and M. Hepting, Magnetic correlations in infinite-layer nickelates: An experimental and theoretical multimethod study, *Phys. Rev. Res.* **4**, 023093 (2022).
- [13] D. Zhao, Y. Zhou, Y. Fu, L. Wang, X. Zhou, H. Cheng, J. Li, D. Song, S. Li, B. Kang, L. Zheng, L. Nie, Z. Wu, M. Shan, F. Yu, J. Ying, S. Wang, J. Mei, T. Wu, and X. Chen, Intrinsic Spin Susceptibility and Pseudogaplike Behavior in Infinite-Layer  $\text{LaNiO}_2$ , *Phys. Rev. Lett.* **126**, 197001 (2021).
- [14] H. Lu, M. Rossi, A. Nag, M. Osada, D. F. Li, K. Lee, B. Y. Wang, M. Garcia-Fernandez, S. Agrestini, Z. X. Shen, E. M. Been, B. Moritz, T. P. Devereaux, J. Zaanen, H. Y. Hwang, K.-J. Zhou, and W. S. Lee, Magnetic excitations in infinite-layer nickelates, *Science* **373**, 213 (2021).
- [15] R. A. Shi, B. Y. Wang, Y. Iguchi, M. Osada, K. Lee, B. H. Goodge, L. F. Kourkoutis, H. Y. Hwang, and K. A. Moler, Scanning SQUID study of ferromagnetism and superconductivity in infinite-layer nickelates, *Phys. Rev. Mater.* **8**, 024802 (2024).
- [16] M. Kitatani, L. Si, O. Janson, R. Arita, Z. Zhong, and K. Held, Nickelate superconductors - a renaissance of the one-band Hubbard model, *npj Quantum Mater.* **5**, 59 (2020).
- [17] F. Lechermann, Assessing the correlated electronic structure of lanthanum nickelates, *Electron. Struct.* **4**, 015005 (2022).
- [18] C.-J. Kang and G. Kotliar, Optical Properties of the Infinite-Layer  $\text{La}_{1-x}\text{Sr}_x\text{NiO}_2$  and Hidden Hund's Physics, *Phys. Rev. Lett.* **126**, 127401 (2021).
- [19] B. Y. Wang, D. Li, B. H. Goodge, K. Lee, M. Osada, S. P. Harvey, L. F. Kourkoutis, M. R. Beasley, and H. Y. Hwang, Isotropic Pauli-limited superconductivity in the infinite-layer nickelate  $\text{Nd}_{0.775}\text{Sr}_{0.225}\text{NiO}_2$ , *Nat. Phys.* **17**, 473 (2021).
- [20] H. Sakakibara, H. Usui, K. Suzuki, T. Kotani, H. Aoki, and K. Kuroki, Model Construction and a Possibility of Cupratelike Pairing in a New  $d^9$  Nickelate Superconductor ( $\text{Nd,Sr}\text{NiO}_2$ ), *Phys. Rev. Lett.* **125**, 077003 (2020).
- [21] X. Wu, D. Di Sante, T. Schwemmer, W. Hanke, H. Y. Hwang, S. Raghu, and R. Thomale, Robust  $d_{x^2-y^2}$ -wave superconductivity of infinite-layer nickelates, *Phys. Rev. B* **101**, 060504 (2020).
- [22] P. Adhikary, S. Bandyopadhyay, T. Das, I. Dasgupta, and T. Saha-Dasgupta, Orbital-selective superconductivity in a two-band model of infinite-layer nickelates, *Phys. Rev. B* **102**, 100501 (2020).
- [23] T. Y. Xie, Z. Liu, C. Cao, Z. F. Wang, J. L. Yang, and W. Zhu, Microscopic theory of superconducting phase diagram in infinite-layer nickelates, *Phys. Rev. B* **106**, 035111 (2022).
- [24] C. Lu, L.-H. Hu, Y. Wang, F. Yang, and C. Wu, Two-orbital model for possible superconductivity pairing mechanism in nickelates, *Phys. Rev. B* **105**, 054516 (2022).
- [25] L. E. Chow, K. Y. Yip, M. Pierre, S. W. Zeng, Z. T. Zhang, T. Heil, J. Deuschle, P. Nandi, Z. S. Lim, Z. Y. Luo, M. Nardone, A. Zitouni, P. A. van Aken, M. Goiran, S. K. Goh, and A. Ariando, Pauli-limit violation in lanthanide infinite-layer nickelate superconductors, *arXiv:2204.12606* (2022).
- [26] W. Wei, W. Sun, Y. Sun, Y. Pan, G. Jin, F. Yang, Y. Li, Z. Zhu, Y. Nie, and Z. Shi, Large upper critical fields and dimensionality crossover of superconductivity in the infinite-layer nickelate  $\text{La}_{0.8}\text{Sr}_{0.2}\text{NiO}_2$ , *Phys. Rev. B* **107**, L220503 (2023).
- [27] S. Yan, W. Mao, W. Sun, Y. Li, H. Sun, J. Yang, B. Hao, W. Guo, L. Nian, Z. Gu, P. Wang, and Y. Nie, Superconductivity in freestanding infinite-layer nickelate membranes (2024).
- [28] B. Y. Wang, T. C. Wang, Y.-T. Hsu, M. Osada, K. Lee, C. Jia, C. Duffy, D. Li, J. Fowlie, M. R. Beasley, T. P. Devereaux, I. R. Fisher, N. E. Hussey, and H. Y. Hwang, Effects of rare-earth magnetism on the superconducting upper critical field in infinite-layer nickelates, *Sci. Adv.* **9**, eadf6655 (2023).
- [29] M.-Y. Choi, K.-W. Lee, and W. E. Pickett, Role of  $4f$  states in infinite-layer  $\text{NdNiO}_2$ , *Phys. Rev. B* **101**, 020503 (2020).
- [30] R. Zhang, C. Lane, B. Singh, J. Nokelainen, B. Barbiellini, R. S. Markiewicz, A. Bansil, and J. Sun, Magnetic and  $f$ -electron effects in  $\text{LaNiO}_2$  and  $\text{NdNiO}_2$  nickelates with cuprate-like  $3d_{x^2-y^2}$  band, *Commun. Phys.* **4**, 118 (2021).
- [31] P. Jiang, L. Si, Z. Liao, and Z. Zhong, Electronic structure of rare-earth infinite-layer  $\text{RNiO}_2$  ( $R = \text{La}, \text{Nd}$ ), *Phys. Rev. B* **100**, 201106 (2019).
- [32] S. Bandyopadhyay, P. Adhikary, T. Das, I. Dasgupta, and T. Saha-Dasgupta, Superconductivity in infinite-layer nickelates: Role of  $f$  orbitals, *Phys. Rev. B* **102**, 220502 (2020).
- [33] D. J. Scalapino, A common thread: The pairing interaction for unconventional superconductors, *Rev. Mod. Phys.* **84**, 1383 (2012).

- [34] Y. Yamakawa, S. Onari, and H. Kontani, Nematicity and Magnetism in FeSe and Other Families of Fe-Based Superconductors, *Phys. Rev. X* **6**, 021032 (2016).
- [35] A. Kreisel, B. M. Andersen, P. O. Sprau, A. Kostin, J. C. S. Davis, and P. J. Hirschfeld, Orbital selective pairing and gap structures of iron-based superconductors, *Phys. Rev. B* **95**, 174504 (2017).
- [36] Y. Wang, C.-J. Kang, H. Miao, and G. Kotliar, Hund's metal physics: From SrNiO<sub>2</sub> to LaNiO<sub>2</sub>, *Phys. Rev. B* **102**, 161118 (2020).
- [37] P. Werner and S. Hoshino, Nickelate superconductors: Multiorbital nature and spin freezing, *Phys. Rev. B* **101**, 041104 (2020).
- [38] J. Krishna, H. LaBollita, A. O. Fumega, V. Pardo, and A. S. Botana, Effects of Sr doping on the electronic and spin-state properties of infinite-layer nickelates: Nature of holes, *Phys. Rev. B* **102**, 224506 (2020).
- [39] I. Leonov, S. L. Skornyakov, and S. Y. Savrasov, Lifshitz transition and frustration of magnetic moments in infinite-layer NdNiO<sub>2</sub> upon hole doping, *Phys. Rev. B* **101**, 241108 (2020).
- [40] W. Sun, Z. Jiang, C. Xia, B. Hao, Y. Li, S. Yan, M. Wang, H. Liu, J. Ding, J. Liu, Z. Liu, J. Liu, H. Chen, D. Shen, and Y. Nie, Title: Electronic structure of superconducting infinite-layer lanthanum nickelates, arxiv:2403.07344 (2024).
- [41] C. Lane, R. Zhang, B. Barbiellini, R. S. Markiewicz, A. Bansil, J. Sun, and J.-X. Zhu, Competing incommensurate spin fluctuations and magnetic excitations in infinite-layer nickelate superconductors, *Commun. Phys.* **6**, 90 (2023).
- [42] Z. Liu, Z. Ren, W. Zhu, Z. Wang, and J. Yang, Electronic and magnetic structure of infinite-layer NdNiO<sub>2</sub>: trace of antiferromagnetic metal, *npj Quantum Mater.* **5**, 31 (2020).
- [43] V. Olevano, F. Bernardini, X. Blase, and A. Cano, *Ab initio* many-body GW correlations in the electronic structure of LaNiO<sub>2</sub>, *Phys. Rev. B* **101**, 161102 (2020).
- [44] See supplemental material at <http://link.aps.org/...> for additional information about the *ab-initio* calculations, derivations of the renormalized superconducting pairing, and results for doped LaNiO<sub>2</sub>, which includes Refs. [18, 20, 23, 34–36, 49, 50, 53, 55, 66–81].
- [45] S. Ryee, H. Yoon, T. J. Kim, M. Y. Jeong, and M. J. Han, Induced magnetic two-dimensionality by hole doping in the superconducting infinite-layer nickelate Nd<sub>1-x</sub>Sr<sub>x</sub>NiO<sub>2</sub>, *Phys. Rev. B* **101**, 064513 (2020).
- [46] A. Kreisel, B. M. Andersen, A. T. Rømer, I. M. Eremin, and F. Lechermann, Superconducting Instabilities in Strongly Correlated Infinite-Layer Nickelates, *Phys. Rev. Lett.* **129**, 077002 (2022).
- [47] K. Kubo, Pairing symmetry in a two-orbital Hubbard model on a square lattice, *Phys. Rev. B* **75**, 224509 (2007).
- [48] H. Tang, M. Plihal, and D. L. Mills, Theory of the spin dynamics of bulk Fe and ultrathin Fe(100) films, *J. Magn. Magn. Mater.* **187**, 23 (1998).
- [49] B. Kang, C. Melnick, P. Semon, S. Ryee, M. J. Han, G. Kotliar, and S. Choi, Infinite-layer nickelates as Ni-*e<sub>g</sub>* Hund's metals, *npj Quantum Mater.* **8**, 35 (2023).
- [50] A. T. Rømer, A. Kreisel, I. Eremin, M. A. Malakhov, T. A. Maier, P. J. Hirschfeld, and B. M. Andersen, Pairing symmetry of the one-band Hubbard model in the paramagnetic weak-coupling limit: A numerical RPA study, *Phys. Rev. B*, 11 (2015).
- [51] P. Worm, Q. Wang, M. Kitatani, I. Bialo, Q. Gao, X. Ren, J. Choi, D. Csontosová, K.-J. Zhou, X. Zhou, Z. Zhu, L. Si, J. Chang, J. M. Tomczak, and K. Held, Spin fluctuations sufficient to mediate superconductivity in nickelates (2023), arXiv:2312.08260.
- [52] N. F. Berk and J. R. Schrieffer, Effect of Ferromagnetic Spin Correlations on Superconductivity, *Phys. Rev. Lett.* **17**, 433 (1966).
- [53] S. Graser, T. A. Maier, P. J. Hirschfeld, and D. J. Scalapino, Near-degeneracy of several pairing channels in multiorbital models for the Fe pnictides, *New J. Phys.* **11**, 025016 (2009).
- [54] A. Kreisel, Y. Wang, T. A. Maier, P. J. Hirschfeld, and D. J. Scalapino, Spin fluctuations and superconductivity in K<sub>x</sub>Fe<sub>2-y</sub>Se<sub>2</sub>, *Phys. Rev. B* **88**, 094522 (2013).
- [55] D. J. Scalapino, E. Loh, and J. E. Hirsch, *d*-wave pairing near a spin-density-wave instability, *Phys. Rev. B* **34**, 8190 (1986).
- [56] M. Dürrnagel, J. Beyer, R. Thomale, and T. Schwemmer, Unconventional superconductivity from weak coupling: A unified perspective on formalism and numerical implementation, *Eur. Phys. J. B* **95**, 112 (2022).
- [57] M. Sigrist, Introduction to Unconventional Superconductivity, *AIP Conf. Proc.* **789**, 165 (2005).
- [58] A. P. Mackenzie and Y. Maeno, The superconductivity of Sr<sub>2</sub>RuO<sub>4</sub> and the physics of spin-triplet pairing, *Rev. Mod. Phys.* **75**, 657 (2003).
- [59] J. W. Serene, The superfluid phases of helium 3, *Science* **251**, 97 (1991).
- [60] M. Sigrist and K. Ueda, Phenomenological theory of unconventional superconductivity, *Rev. Mod. Phys.* **63**, 239 (1991).
- [61] J. F. Annett, B. L. Györfy, and K. I. Wysokiński, Orbital magnetic moment of a chiral *p*-wave superconductor, *New J. Phys.* **11**, 055063 (2009).
- [62] M. P. Smylie, H. Claus, U. Welp, W.-K. Kwok, Y. Qiu, Y. S. Hor, and A. Snezhko, Evidence of nodes in the order parameter of the superconducting doped topological insulator Nb<sub>x</sub>Bi<sub>2</sub>Se<sub>3</sub> via penetration depth measurements, *Phys. Rev. B* **94**, 180510 (2016).
- [63] R. T. Gordon, C. Martin, H. Kim, N. Ni, M. A. Tanatar, J. Schmalian, I. I. Mazin, S. L. Bud'ko, P. C. Canfield, and R. Prozorov, London penetration depth in single crystals of Ba(Fe<sub>1-x</sub>Co<sub>x</sub>)<sub>2</sub>As<sub>2</sub> spanning underdoped to overdoped compositions, *Phys. Rev. B* **79**, 100506 (2009).
- [64] S. P. Harvey, B. Y. Wang, J. Fowlie, M. Osada, K. Lee, Y. Lee, D. Li, and H. Y. Hwang, Evidence for nodal superconductivity in infinite-layer nickelates, arXiv:2201.12971 (2022).
- [65] L. E. Chow, S. K. Sudheesh, Z. Y. Luo, P. Nandi, T. Heil, J. Deuschle, S. W. Zeng, Z. T. Zhang, S. Prakash, X. M. Du, Z. S. Lim, P. A. van Aken, E. E. M. Chia, and A. Ariando, Pairing symmetry in infinite-layer nickelate superconductors, arXiv:2201.10038 (2023).
- [66] G. Kresse and D. Joubert, From ultrasoft pseudopotentials to the projector augmented-wave method, *Phys. Rev. B* **59**, 1758 (1999).
- [67] G. Kresse and J. Furthmüller, Efficient iterative schemes for *ab initio* total-energy calculations using a plane-wave basis set, *Phys. Rev. B* **54**, 11169 (1996).
- [68] J. P. Perdew, J. A. Chevary, S. H. Vosko, K. A. Jackson, M. R. Pederson, D. J. Singh, and C. Fiolhais, Atoms, molecules, solids, and surfaces: Applications of the gen-

- eralized gradient approximation for exchange and correlation, Phys. Rev. B **46**, 6671 (1992).
- [69] A. D. Becke, Density-functional exchange-energy approximation with correct asymptotic behavior, Phys. Rev. A **38**, 3098 (1988).
- [70] D. C. Langreth and M. J. Mehl, Beyond the local-density approximation in calculations of ground-state electronic properties, Phys. Rev. B **28**, 1809 (1983).
- [71] P. E. Blöchl, Projector augmented-wave method, Phys. Rev. B **50**, 17953 (1994).
- [72] J. P. Perdew, K. Burke, and M. Ernzerhof, Generalized gradient approximation made simple, Phys. Rev. Lett. **77**, 3865 (1996).
- [73] G. H. Wannier, The structure of electronic excitation levels in insulating crystals, Phys. Rev. **52**, 191 (1937).
- [74] G. H. Wannier, Dynamics of band electrons in electric and magnetic fields, Rev. Mod. Phys. **34**, 645 (1962).
- [75] A. A. Mostofi, J. R. Yates, G. Pizzi, Y.-S. Lee, I. Souza, D. Vanderbilt, and N. Marzari, An updated version of wannier90: A tool for obtaining maximally-localised wannier functions, Comp. Phys. Commun. **185**, 2309 (2014).
- [76] N. Marzari, A. A. Mostofi, J. R. Yates, I. Souza, and D. Vanderbilt, Maximally localized wannier functions: Theory and applications, Rev. Mod. Phys. **84**, 1419 (2012).
- [77] N. Marzari and D. Vanderbilt, Maximally localized generalized wannier functions for composite energy bands, Phys. Rev. B **56**, 12847 (1997).
- [78] I. Souza, N. Marzari, and D. Vanderbilt, Maximally localized wannier functions for entangled energy bands, Phys. Rev. B **65**, 035109 (2001).
- [79] V. Wang, N. Xu, J.-C. Liu, G. Tang, and W.-T. Geng, Vaspkit: A user-friendly interface facilitating high-throughput computing and analysis using vasp code, Comp. Phys. Commun. **267**, 108033 (2021).
- [80] K. Momma and F. Izumi, *VESTA*: a three-dimensional visualization system for electronic and structural analysis, Journ. Appl. Cryst. **41**, 653 (2008).
- [81] A. F. Kemper, T. A. Maier, S. Graser, H.-P. Cheng, P. J. Hirschfeld, and D. J. Scalapino, Sensitivity of the superconducting state and magnetic susceptibility to key aspects of electronic structure in ferropnictides, New J. Phys. **12**, 073030 (2010).



# Supplemental Material: Orbital-Selective Spin-Triplet Superconductivity in Infinite-Layer Lanthanum Nickelates

Fabian Jakubczyk,<sup>1,2</sup> Armando Consiglio,<sup>3,2</sup> Domenico Di Sante,<sup>4</sup> Ronny Thomale,<sup>3,2</sup> and Carsten Timm<sup>1,2</sup>

<sup>1</sup>*Institute of Theoretical Physics, Technische Universität Dresden, 01069 Dresden, Germany*

<sup>2</sup>*Würzburg-Dresden Cluster of Excellence ct.qmat, Germany*

<sup>3</sup>*Institut für Theoretische Physik und Astrophysik, Universität Würzburg, 97074 Würzburg, Germany*

<sup>4</sup>*Department of Physics and Astronomy, University of Bologna, 40127 Bologna, Italy*

(Dated: March 29, 2024)

## I. DFT ELECTRONIC STRUCTURE AND WANNIER HAMILTONIAN

DFT calculations have been performed using the Vienna ab-initio Simulation Package (VASP) [1, 2], employing the projector augmented wave (PAW) method [3]. Exchange and correlation effects have been handled using the generalized gradient approximation (GGA) [4–6] within the Perdew-Burke-Ernzerhof (PBE) approach [7]. A plane-wave cutoff of 500 eV was used for the truncation of the basis set, while the relaxation of the electronic and ionic degrees of freedom was considered converged when the output difference between two steps was equal or smaller than  $1 \times 10^{-6}$  eV and  $1 \times 10^{-8}$  eV/Å, respectively. The chosen number of  $\mathbf{k}$ -points is  $16 \times 16 \times 16$ . Partial occupancies have been determined via Gaussian smearing with a width of 0.1 eV. Spin-orbit coupling (SOC) has generally not been considered, unless stated otherwise, in which case SOC has been included self-consistently. The comparison between the cases with and without SOC is shown in Fig. S1(d). Subsequently, Wannier functions [8, 9] have been used to provide an equivalent description of Bloch states via a maximally localized orbital basis. The Wannier-basis position matrix elements  $\langle 0n|\hat{r}|Rm\rangle$ ,  $Rm$  being the maximally-localized Wannier function  $m$  in unit cell  $R$ , have been used for the tight-binding description, as shown in Figs. S1(a) and S1(b) [10–13]. For the three-band model, the projection functions used to build the initial guess  $A(\mathbf{k})_{mn} = \langle \psi_{m\mathbf{k}}|g_n\rangle$  for the unitary transformation are provided by Ni  $d_{x^2-y^2}$ , La  $d_{xy}$ , and La  $d_{z^2}$  orbitals.  $|g_n\rangle$  represents the trial localized orbitals, and  $|\psi_{m\mathbf{k}}\rangle$  are the Bloch states. DFT band structures have been visualized using the VASPKIT postprocessing tool, as shown in Fig. S1(c) [14], while VESTA [15] has been used to visualize the Wannier-orbital isosurfaces and crystal structures in Fig. S1(a).

We introduce the operator  $\psi_{\sigma}^{\dagger}(\mathbf{k}) = [c_{1\sigma}^{\dagger}(\mathbf{k}), c_{2\sigma}^{\dagger}(\mathbf{k}), c_{3\sigma}^{\dagger}(\mathbf{k})]$  to describe the given multiband system. Here,  $c_{l\sigma}^{\dagger}(\mathbf{k})$  is the fermionic creation operator, where  $\sigma$  and  $l$  denote the spin and orbital index, with  $l = 1, 2, 3$  referring to the La  $5d_{z^2}$ , La  $5d_{xy}$ , and Ni  $3d_{x^2-y^2}$  orbital, respectively. We thus write the non-interacting Hamiltonian as

$$H_0 = \sum_{\mathbf{k}\sigma} \psi_{\sigma}^{\dagger}(\mathbf{k}) h(\mathbf{k}) \psi_{\sigma}(\mathbf{k}). \quad (\text{S1})$$

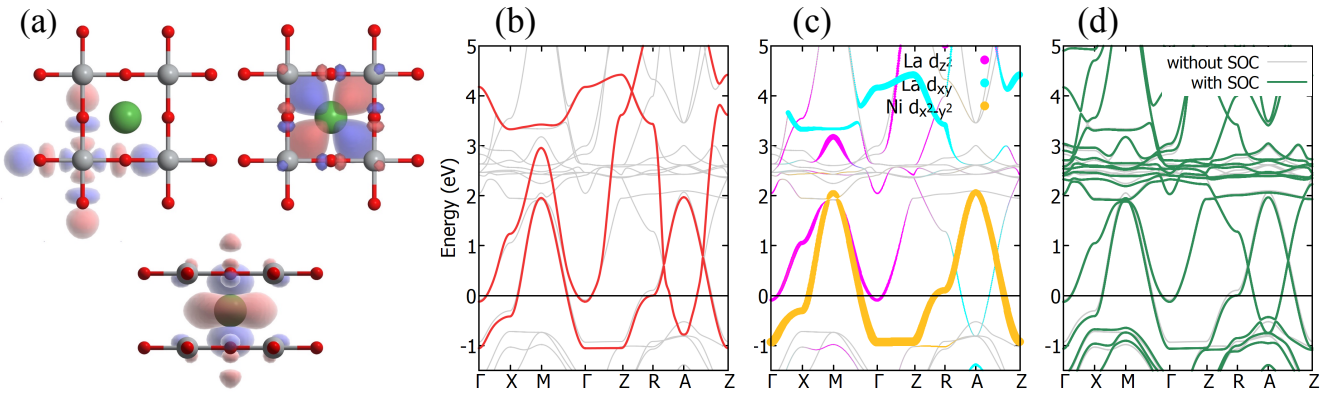


FIG. S1. (a) Isosurfaces of the Wannier orbitals used for the three-band model. The upper left and right panels show top views of the Ni  $d_{x^2-y^2}$  and La  $d_{xy}$  Wannier orbitals, respectively. The lower panel shows a side view of the La  $d_{z^2}$  orbital. (b) Comparison between DFT band structure (gray lines) and bands derived from the three-band Wannier model (red lines). (c) DFT band structure projected onto the three orbitals of the model: La  $d_{z^2}$ , La  $d_{xy}$ , and Ni  $d_{x^2-y^2}$ . (d) Comparison between DFT band structures, with and without SOC.

For the derivation of the matrix elements in the Hamiltonian  $h(\mathbf{k})$  we employ an energy cutoff of 0.01 eV for the tight-binding (TB) hopping amplitudes. The Hamiltonian is given by

$$h_{11} = \epsilon_1 - \mu + 2t_{11}^x (\cos k_x + \cos k_y + 2t_{11}^{xx} (\cos 2k_x + \cos 2k_y) + 2t_{11}^z \cos k_z + 2t_{11}^{zz} \cos 2k_z) + 4t_{11}^{zz} \cos 2k_z (\cos k_x + \cos k_y), \quad (\text{S2})$$

$$\begin{aligned} h_{22} = & \epsilon_2 - \mu + 2t_{22}^x (\cos k_x + \cos k_y) + 4t_{22}^{xy} \cos k_x \cos k_y + 2t_{22}^{xx} (\cos 2k_x + \cos 2k_y) \\ & + 4t_{22}^{xy} (\cos 2k_x \cos k_y + \cos k_x \cos 2k_y) + 2t_{22}^z \cos k_z + 2t_{22}^{zz} \cos 2k_z \\ & + 4t_{22}^{zz} \cos k_z (\cos k_x + \cos k_y) + 8t_{22}^{xyz} \cos k_x \cos k_y \cos k_z + 4t_{22}^{xzz} \cos k_z (\cos 2k_x + \cos 2k_y) \\ & + 8t_{22}^{xyzz} \cos k_z (\cos 2k_x \cos k_y + \cos k_x \cos 2k_y) + 2t_{22}^{zzz} \cos(3k_z) \\ & + 4t_{22}^{zzz} \cos 2k_z (\cos k_x + \cos k_y) + 4t_{22}^{xzzz} \cos 2k_z (\cos 2k_x + \cos 2k_y) \\ & + 8t_{22}^{xyzzz} \cos 2k_z (\cos 2k_x \cos k_y + \cos k_x \cos 2k_y), \end{aligned} \quad (\text{S3})$$

$$h_{33} = \epsilon_3 - \mu + 2t_{33}^x (\cos k_x + \cos k_y) + 4t_{33}^{xy} \cos k_x \cos k_y + 2t_{33}^{xx} (\cos 2k_x + \cos 2k_y) + 2t_{33}^z \cos k_z + 8t_{33}^{xyz} \cos k_x \cos k_y \cos k_z, \quad (\text{S4})$$

$$h_{12} = -4t_{12}^{xy} \sin k_x \sin k_y - 8t_{12}^{xyz} \sin k_x \sin k_y \cos k_z - 8t_{12}^{xyzz} \sin k_x \sin k_y \cos 2k_z, \quad (\text{S5})$$

$$h_{13} = 8t_{13}^x (\cos 3/2k_x \cos 1/2k_y - \cos 1/2k_x \cos 3/2k_y) \cos 1/2k_z + 8t_{13}^z (\cos 3/2k_x \cos 1/2k_y - \cos 1/2k_x \cos 3/2k_y) \cos 3/2k_z, \quad (\text{S6})$$

$$h_{23} = -8t_{23}^x (\sin 3/2k_x \sin 1/2k_y - \sin 1/2k_x \sin 3/2k_y) \cos 1/2k_z - 8t_{23}^z (\sin 3/2k_x \sin 1/2k_y - \sin 1/2k_x \sin 3/2k_y) \cos 3/2k_z. \quad (\text{S7})$$

We use a chemical potential of  $\mu = 9.28$  eV and  $\mu = 9.12$  eV in the undoped and doped scenario, respectively. The corresponding TB parameters specified in unit of eV are

$$\epsilon_1 = 12.3837, \quad \epsilon_2 = 12.3325, \quad \epsilon_3 = 9.6706, \quad (\text{S8})$$

$$t_{11}^x = -0.4266, \quad t_{11}^{xx} = 0.0401, \quad t_{11}^z = -1.0314, \quad t_{11}^{zz} = 0.1150, \quad t_{11}^{xzz} = 0.0155, \quad (\text{S9})$$

$$t_{22}^x = 0.3964, \quad t_{22}^{xy} = -0.0602, \quad t_{22}^{xx} = 0.0417, \quad t_{22}^z = 0.3545, \quad t_{22}^{zz} = -0.1680, \quad t_{22}^{xyz} = 0.0571,$$

$$t_{22}^{zz} = -0.0549, \quad t_{22}^{xzz} = -0.0242, \quad t_{22}^{xyy} = -0.0230, \quad t_{22}^{xyyz} = 0.0210, \quad t_{22}^{zzz} = 0.0113, \\ t_{22}^{zzz} = 0.0144, \quad t_{22}^{xzzz} = 0.0103, \quad t_{22}^{xyzzz} = -0.0107, \quad (\text{S10})$$

$$t_{33}^x = -0.3656, \quad t_{33}^{xy} = 0.0941, \quad t_{33}^{xx} = -0.0441, \quad t_{33}^z = -0.0413, \quad t_{33}^{xyz} = 0.0121, \quad (\text{S11})$$

$$t_{12}^{xy} = 0.0777, \quad t_{12}^{xyz} = -0.0541, \quad t_{12}^{xyzz} = 0.0100, \quad (\text{S12})$$

$$t_{13}^x = 0.0277, \quad t_{13}^z = -0.0142, \quad (\text{S13})$$

$$t_{23}^x = -0.0183, \quad t_{23}^z = 0.0198. \quad (\text{S14})$$

The density of states (DOS) of the unrenormalized system can be obtained from

$$\rho(\omega_n) = -\frac{1}{N\pi} \sum_{\mathbf{k}} \text{Im} \text{Tr}[(i\omega_n \mathbb{1} - h(\mathbf{k}))^{-1}]. \quad (\text{S15})$$

## II. RENORMALIZED SUSCEPTIBILITIES AND SUPERCONDUCTING PAIRING

Within the orbital selective ansatz [16, 17], quasiparticles in orbital  $l$  are weighted by a factor  $\sqrt{Z_l}$ , i.e.,  $c_l^\dagger(\mathbf{k}) \rightarrow \sqrt{Z_l} c_l^\dagger(\mathbf{k})$ , such that the Green's function in the orbital basis  $G_{ll'}(\mathbf{k}, \omega_n)$  becomes

$$\tilde{G}_{ll'}(\mathbf{k}, \omega_n) = \sqrt{Z_l Z_{l'}} \sum_{\mu} \frac{a_{\mu}^l(\mathbf{k}) a_{\mu}^{l'*}(\mathbf{k})}{i\omega_n - E_{\mu}(\mathbf{k})}, \quad (\text{S16})$$

where  $E_{\mu}(\mathbf{k})$  is the eigenenergy of band  $\mu$ . The renormalized Green's function enters the bare (non-interacting) susceptibilities, which after performing Matsubara-frequency summation read as

$$\tilde{\chi}_{l_1 l_2 l_3 l_4}^0(\mathbf{q}, \omega) = -\frac{1}{N} \sum_{\mathbf{k}, \mu\nu} \tilde{\eta}_{\mu\nu}(\mathbf{k}, \mathbf{q}) \frac{n_F(E_{\nu}(\mathbf{k} + \mathbf{q})) - n_F(E_{\mu}(\mathbf{k}))}{E_{\nu}(\mathbf{k} + \mathbf{q}) - E_{\mu}(\mathbf{k}) + \omega + i0^+}, \quad (\text{S17})$$

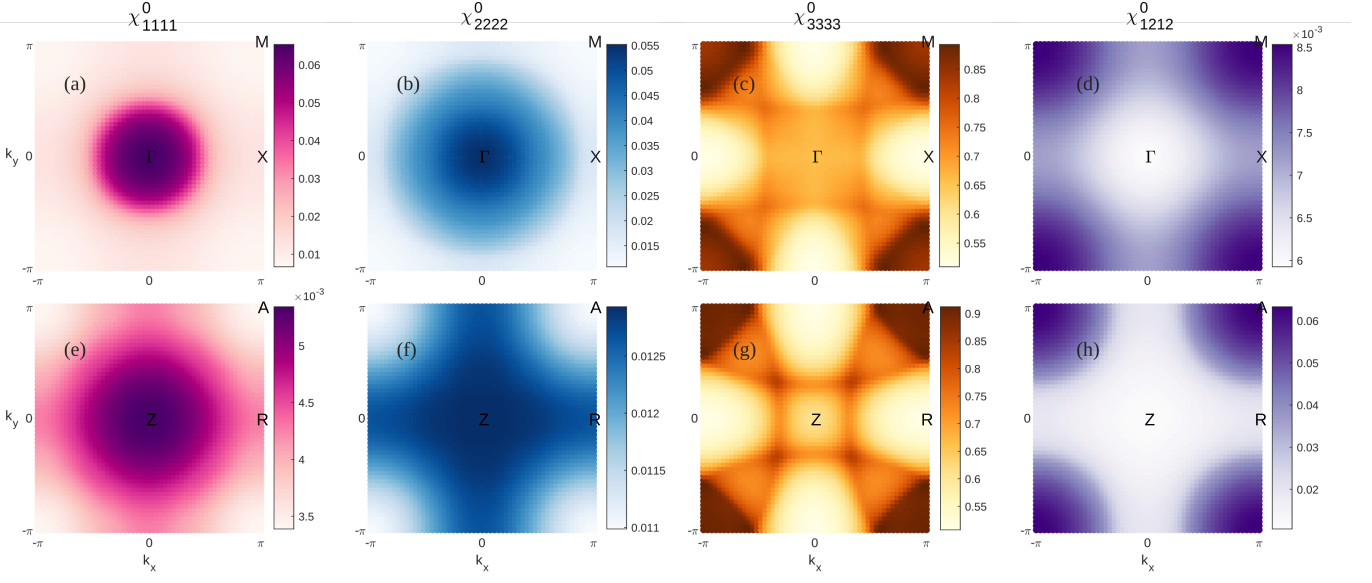


FIG. S2. Static ( $\omega = 0$ ) bare susceptibilities of pristine LaNiO<sub>2</sub> for  $Z_{d_{x^2-y^2}} = 1$  in the  $k_x$   $k_y$ -plane for (a) - (d)  $k_z = 0$  and (e) - (h)  $k_z = \pi$ . In panels (a), (e)  $\tilde{\chi}_{1111}^0$ , (b), (f)  $\tilde{\chi}_{2222}^0$ , and (c), (g)  $\tilde{\chi}_{3333}^0$  represent the diagonal La  $d_{z^2}$ , La  $d_{xy}$ , and Ni  $d_{x^2-y^2}$  orbital contributions, respectively. Moreover, we show the off-diagonal  $\tilde{\chi}_{1212}^0$  susceptibility in panels (d) & (h). Momentum space integration is done on a mesh of  $60 \times 60 \times 60$   $\mathbf{k}$ -points.

with the Fermi-Dirac distribution  $n_F$ . Here, we have absorbed the quasiparticle weights into the dressing factor

$$\tilde{\eta}_{\mu\nu}(\mathbf{k}, \mathbf{q}) = \sqrt{Z_{l_1} Z_{l_2} Z_{l_3} Z_{l_4}} a_{\mu}^{l_4}(\mathbf{k}) a_{\mu}^{l_2*}(\mathbf{k}) a_{\nu}^{l_1}(\mathbf{k} + \mathbf{q}) a_{\nu}^{l_3*}(\mathbf{k} + \mathbf{q}), \quad (\text{S18})$$

and  $a_{\mu}^l(\mathbf{k})$  is the matrix element of the unitary transformation that connects band  $\mu$  to orbital  $l$ . The homogeneous or physical bare spin susceptibility can be calculated by performing the sum

$$\tilde{\chi}_{\text{phys}}^0(\mathbf{q}) = \frac{1}{2} \sum_w \tilde{\chi}_{ll'vw}^0(\mathbf{q}, 0) \quad (\text{S19})$$

of the static ( $\omega = 0$ ) susceptibility [18]. In Fig. S2, we show plots of the bare susceptibilities  $\tilde{\chi}_{1111}^0$ ,  $\tilde{\chi}_{2222}^0$ ,  $\tilde{\chi}_{3333}^0$ , and  $\tilde{\chi}_{1212}^0$  obtained for undoped LaNiO<sub>2</sub> without renormalization along 2D cuts ( $k_z = 0, \pi$ ) through the Brillouin zone (BZ). Especially the  $\tilde{\chi}_{3333}^0$  component shows nesting features familiar from the cuprates [19]. However, quasiparticle renormalization strongly dampens these features, such that they become less significant in the renormalized case. Note that for instance the off-diagonal  $\tilde{\chi}_{1212}^0$  susceptibility contribution would not be observable within the physical susceptibility given in Eq. (S19).

Interactions are included in the calculation of susceptibilities within the random phase approximation (RPA). The spin-fluctuation and charge-fluctuation parts of the susceptibility are then given by [20]

$$\tilde{\chi}_{l_1 l_2 l_3 l_4}^{\text{RPA}, s}(\mathbf{q}, \omega) = \{\tilde{\chi}^0(\mathbf{q}, \omega) [\mathbb{1} - U^s \tilde{\chi}^0(\mathbf{q}, \omega)]\}_{l_1 l_2 l_3 l_4}^{-1}, \quad (\text{S20})$$

$$\tilde{\chi}_{l_1 l_2 l_3 l_4}^{\text{RPA}, c}(\mathbf{q}, \omega) = \{\tilde{\chi}^0(\mathbf{q}, \omega) [\mathbb{1} + U^c \tilde{\chi}^0(\mathbf{q}, \omega)]\}_{l_1 l_2 l_3 l_4}^{-1}. \quad (\text{S21})$$

In orbital space, the spin and charge interaction matrices  $U^s$  and  $U^c$  containing the interaction parameters are given by

$$U_{l_1 l_2 l_3 l_4}^s = \begin{cases} U_{\tau}, & l_1 = l_2 = l_3 = l_4, \\ U'_{\tau}, & l_1 = l_3 \neq l_2 = l_4, \\ J_{\tau}, & l_1 = l_2 \neq l_3 = l_4, \\ J'_{\tau}, & l_1 = l_4 \neq l_2 = l_3, \end{cases} \quad (\text{S22})$$

$$U_{l_1 l_2 l_3 l_4}^c = \begin{cases} U_{\tau}, & l_1 = l_2 = l_3 = l_4, \\ -U'_{\tau} + 2J_{\tau}, & l_1 = l_3 \neq l_2 = l_4, \\ 2U'_{\tau} - J_{\tau}, & l_1 = l_2 \neq l_3 = l_4, \\ J'_{\tau}, & l_1 = l_4 \neq l_2 = l_3, \end{cases} \quad (\text{S23})$$

respectively, where  $\tau \in (\text{La}, \text{Ni})$  is the sublattice index.

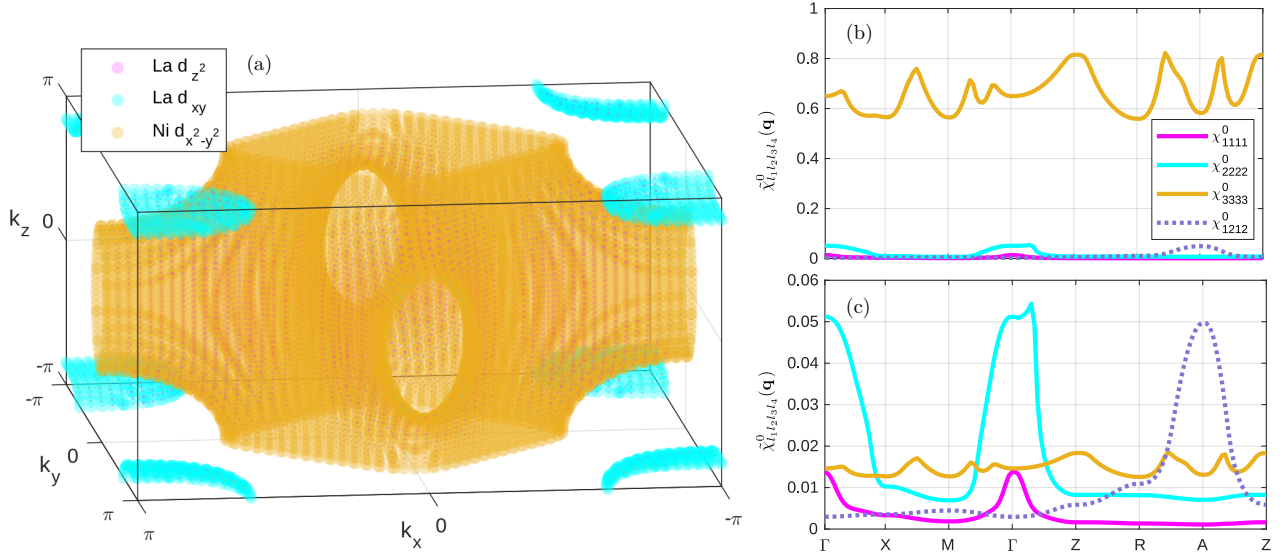


FIG. S3. (a) 3D Fermi surface including the orbital contributions relevant for the low-energy description of doped LaNiO<sub>2</sub>. Magenta, cyan, and yellow refer to the La  $d_{z^2}$ , La  $d_{xy}$ , and Ni  $d_{x^2-y^2}$  orbitals, respectively. (b), (c) Static bare susceptibilities  $\tilde{\chi}_{l_1 l_2 l_3 l_4}^0(\mathbf{q}, \omega = 0)$  for (b)  $Z_{d_{x^2-y^2}} = 1$  and (c)  $Z_{d_{x^2-y^2}} = 0.15$  for doped LaNiO<sub>2</sub>. The off-diagonal bare susceptibility  $\tilde{\chi}_{1212}^0$  is shown in purple. The mesh for momentum space integration includes  $80 \times 80 \times 80$   $\mathbf{k}$ -points.

In order to determine the superconducting (SC) pairing symmetries, we solve the linearized gap equation

$$\lambda_\alpha f_\alpha(\mathbf{k}) = \sum_j \oint_{C_j} \frac{d^2 k'_\parallel}{(2\pi)^2 v_F(\mathbf{k}')} \tilde{\Gamma}_{ij}(\mathbf{k}, \mathbf{k}') f_\alpha(\mathbf{k}'). \quad (\text{S24})$$

The largest eigenvalue  $\lambda_\alpha$  of equation (S24) results in the highest transition temperature [18], while  $\lambda_\alpha$  in general determines the pairing strength for the different pairing channels  $\alpha$  [21]. The corresponding gap symmetries are identified by the eigenfunction  $f_\alpha(\mathbf{k})$ . The inverse Fermi velocity  $v_F(\mathbf{k}) = |\nabla_{\mathbf{k}} E_\nu(\mathbf{k})|$  gives a measure of the DOS and momenta  $\mathbf{k} \in C_i$ ,  $\mathbf{k}' \in C_j$  are constrained to the FS sheets  $C_{i,j}$ . In Eq. (S24),  $\tilde{\Gamma}_{ij}(\mathbf{k}, \mathbf{k}')$  represents the renormalized form of the effective multiorbital pair scattering vertex and is given by

$$\tilde{\Gamma}_{ij}(\mathbf{k}, \mathbf{k}') = \text{Re} \sum_{l_1 l_2 l_3 l_4} \sqrt{Z_{l_1}} \sqrt{Z_{l_4}} a_{\nu_i}^{l_1, *}(\mathbf{k}) a_{\nu_i}^{l_4, *}(-\mathbf{k}) \tilde{\Gamma}_{l_1 l_2 l_3 l_4}^{S/T}(\mathbf{k}, \mathbf{k}', \omega = 0) \sqrt{Z_{l_2}} \sqrt{Z_{l_3}} a_{\nu_j}^{l_2}(\mathbf{k}') a_{\nu_j}^{l_3}(-\mathbf{k}'), \quad (\text{S25})$$

$$\tilde{\Gamma}_{l_1 l_2 l_3 l_4}^S(\mathbf{k}, \mathbf{k}', \omega) = \left[ \frac{3}{2} U^s \tilde{\chi}_{l_1 l_2 l_3 l_4}^{\text{RPA}, s}(\mathbf{k} - \mathbf{k}') U^s + \frac{1}{2} U^s - \frac{1}{2} U^c \tilde{\chi}_{l_1 l_2 l_3 l_4}^{\text{RPA}, c}(\mathbf{k} - \mathbf{k}') U^c + \frac{1}{2} U^c \right]_{l_1 l_2 l_3 l_4}, \quad (\text{S26})$$

$$\tilde{\Gamma}_{l_1 l_2 l_3 l_4}^T(\mathbf{k}, \mathbf{k}', \omega) = \left[ -\frac{1}{2} U^s \tilde{\chi}_{l_1 l_2 l_3 l_4}^{\text{RPA}, s}(\mathbf{k} - \mathbf{k}') U^s + \frac{1}{2} U^s - \frac{1}{2} U^c \tilde{\chi}_{l_1 l_2 l_3 l_4}^{\text{RPA}, c}(\mathbf{k} - \mathbf{k}') U^c + \frac{1}{2} U^c \right]_{l_1 l_2 l_3 l_4}. \quad (\text{S27})$$

Here,  $\tilde{\Gamma}_{l_1 l_2 l_3 l_4}$  determines the orbital vertex functions in the singlet ( $S$ ) and triplet ( $T$ ) channel. Physically,  $\tilde{\Gamma}_{l_1 l_2 l_3 l_4}$  reflects particle-particle scattering of electrons from orbitals  $l_1, l_4$  into orbitals  $l_2, l_3$ . The quantities  $U^s, U^c, \chi^{\text{RPA}}$  are matrices in orbital space and  $\chi^{\text{RPA}, s/c}$  describes spin or charge fluctuations, respectively.

### III. DOPED LaNiO<sub>2</sub>

A natural question is whether the observed odd-parity  $p$ -wave state is also realized in doped LaNiO<sub>2</sub>. To investigate this, we capture the essential impact of doping by a rigid shift of the chemical potential, such that the  $\Gamma$ -centered electron pocket is lifted above the Fermi level. We show the corresponding 3D FS in Fig. S3(a).

In the next step, we analyze the bare susceptibilities shown in Figs. S3(b) and S3(c). On the one hand, the diagonal susceptibility  $\tilde{\chi}_{3333}^0$  loses its main peaks around the A and M points and becomes almost featureless, fluctuating around an amplitude of  $\tilde{\chi}_{3333}^0 \approx 0.7$  in the unrenormalized case. On the other hand, once we introduce correlations by setting  $Z_{d_{x^2-y^2}} = 0.15$  like

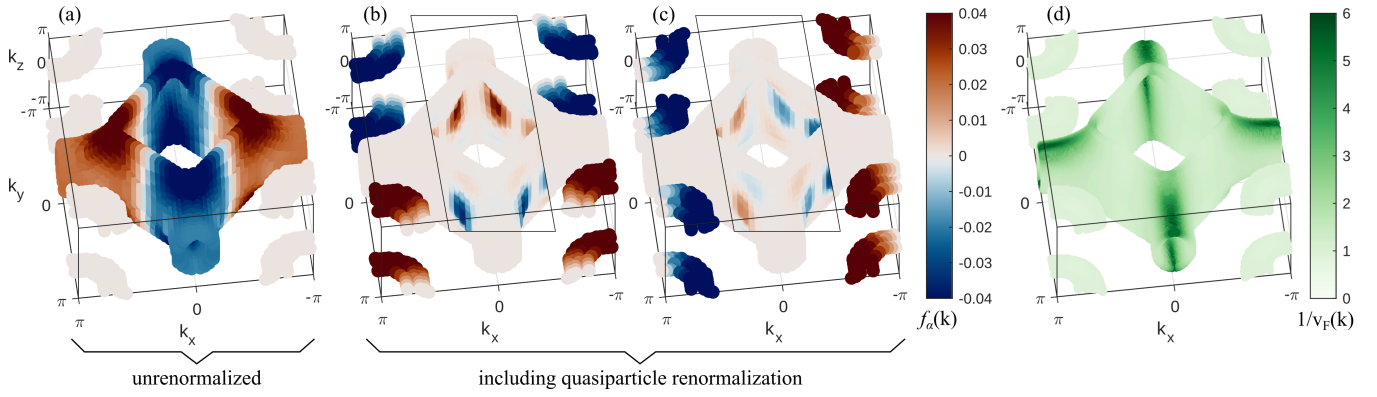


FIG. S4. Leading pairing structure of doped LaNiO<sub>2</sub> with and without inclusion of quasiparticle renormalization for (a)  $Z_{d_{x^2-y^2}} = 1$  and (b), (c)  $Z_{d_{x^2-y^2}} = 0.15$ . The gap symmetry transitions from (a) an even-parity  $d$ -wave to (b), (c) a degenerate odd-parity  $p$ -wave solution. A colorscale highlighting smaller amplitudes with maximum value of  $\pm 1 \times 10^{-4}$  was chosen for the insets to reveal the sign change on the large FS as a function of  $k_z$ . In (d) the momentum-dependent inverse Fermi-velocity  $1/v_F(\mathbf{k}) = 1/|\nabla_{\mathbf{k}} E_{\nu}(\mathbf{k})|$  gives a measure of the DOS.

in the main text, the central features are again given by the diagonal rare-earth contributions  $\tilde{\chi}_{1111}^0$  and  $\tilde{\chi}_{2222}^0$  around  $\Gamma$ , as well as the off-diagonal component  $\tilde{\chi}_{1212}^0$  around A. In contrast to undoped LaNiO<sub>2</sub>, the diagonal La  $d_{xy}$  susceptibility  $\tilde{\chi}_{2222}^0$  now far surpasses  $\tilde{\chi}_{1111}^0$  from the La  $d_{z^2}$  orbital. This is not surprising since La  $d_{z^2}$  electrons used to contribute mainly to the pocket around  $\Gamma$ , which has vanished due to doping.

Finally, we also perform calculations of the pairing symmetry in doped LaNiO<sub>2</sub>, which can be seen in Fig. S4. Most interestingly, we observe that the essential conclusions made for the SC state of the undoped compound are still valid. The gap now clearly dominates on the remaining rare-earth pockets around A. In fact, the transition to a favored  $p$ -wave happens for even bigger quasiparticle weights of  $Z_{d_{x^2-y^2}} \lesssim 0.3$ , which might be facilitated due to a reduced DOS at the van Hove features around R. Note that a decreased mass enhancement due to doping might have a compensating effect. Like in the case of undoped LaNiO<sub>2</sub>, we set  $U_{\text{Ni}} = 5$  eV for the renormalized calculations and  $U_{\text{Ni}} = 0.5$  eV for  $Z_{d_{x^2-y^2}} = 1$ . Furthermore, we again applied  $U_{\text{La}}/U_{\text{Ni}} = 0.5$  and  $J_{\text{La}}/U_{\text{La}} = 0.2$  [22–26].

- 
- [1] G. Kresse and D. Joubert, From ultrasoft pseudopotentials to the projector augmented-wave method, Phys. Rev. B **59**, 1758 (1999).
  - [2] G. Kresse and J. Furthmüller, Efficient iterative schemes for ab initio total-energy calculations using a plane-wave basis set, Phys. Rev. B **54**, 11169 (1996).
  - [3] P. E. Blöchl, Projector augmented-wave method, Phys. Rev. B **50**, 17953 (1994).
  - [4] J. P. Perdew, J. A. Chevary, S. H. Vosko, K. A. Jackson, M. R. Pederson, D. J. Singh, and C. Fiolhais, Atoms, molecules, solids, and surfaces: Applications of the generalized gradient approximation for exchange and correlation, Phys. Rev. B **46**, 6671 (1992).
  - [5] A. D. Becke, Density-functional exchange-energy approximation with correct asymptotic behavior, Phys. Rev. A **38**, 3098 (1988).
  - [6] D. C. Langreth and M. J. Mehl, Beyond the local-density approximation in calculations of ground-state electronic properties, Phys. Rev. B **28**, 1809 (1983).
  - [7] J. P. Perdew, K. Burke, and M. Ernzerhof, Generalized gradient approximation made simple, Phys. Rev. Lett. **77**, 3865 (1996).
  - [8] G. H. Wannier, The structure of electronic excitation levels in insulating crystals, Phys. Rev. **52**, 191 (1937).
  - [9] G. H. Wannier, Dynamics of band electrons in electric and magnetic fields, Rev. Mod. Phys. **34**, 645 (1962).
  - [10] A. A. Mostofi, J. R. Yates, G. Pizzi, Y.-S. Lee, I. Souza, D. Vanderbilt, and N. Marzari, An updated version of wannier90: A tool for obtaining maximally-localised wannier functions, Comp. Phys. Commun. **185**, 2309 (2014).
  - [11] N. Marzari, A. A. Mostofi, J. R. Yates, I. Souza, and D. Vanderbilt, Maximally localized wannier functions: Theory and applications, Rev. Mod. Phys. **84**, 1419 (2012).
  - [12] N. Marzari and D. Vanderbilt, Maximally localized generalized wannier functions for composite energy bands, Phys. Rev. B **56**, 12847 (1997).
  - [13] I. Souza, N. Marzari, and D. Vanderbilt, Maximally localized wannier functions for entangled energy bands, Phys. Rev. B **65**, 035109 (2001).
  - [14] V. Wang, N. Xu, J.-C. Liu, G. Tang, and W.-T. Geng, Vaspkit: A user-friendly interface facilitating high-throughput computing and analysis using vasp code, Comp. Phys. Commun. **267**, 108033 (2021).
  - [15] K. Momma and F. Izumi, VESTA: a three-dimensional visualization system for electronic and structural analysis, Journ. Appl. Cryst. **41**, 653 (2008).
  - [16] Y. Yamakawa, S. Onari, and H. Kontani, Nematicity and Magnetism in FeSe and Other Families of Fe-Based Superconductors, Phys.

- Rev. X **6**, 021032 (2016).
- [17] A. Kreisel, B. M. Andersen, P. O. Sprau, A. Kostin, J. C. S. Davis, and P. J. Hirschfeld, Orbital selective pairing and gap structures of iron-based superconductors, *Phys. Rev. B* **95**, 174504 (2017).
  - [18] S. Graser, T. A. Maier, P. J. Hirschfeld, and D. J. Scalapino, Near-degeneracy of several pairing channels in multiorbital models for the Fe pnictides, *New J. Phys.* **11**, 025016 (2009).
  - [19] A. T. Rømer, A. Kreisel, I. Eremin, M. A. Malakhov, T. A. Maier, P. J. Hirschfeld, and B. M. Andersen, Pairing symmetry of the one-band Hubbard model in the paramagnetic weak-coupling limit: A numerical RPA study, *Phys. Rev. B* , 11 (2015).
  - [20] A. F. Kemper, T. A. Maier, S. Graser, H.-P. Cheng, P. J. Hirschfeld, and D. J. Scalapino, Sensitivity of the superconducting state and magnetic susceptibility to key aspects of electronic structure in ferropnictides, *New J. Phys.* **12**, 073030 (2010).
  - [21] D. J. Scalapino, E. Loh, and J. E. Hirsch, *d*-wave pairing near a spin-density-wave instability, *Phys. Rev. B* **34**, 8190 (1986).
  - [22] H. Sakakibara, H. Usui, K. Suzuki, T. Kotani, H. Aoki, and K. Kuroki, Model Construction and a Possibility of Cupratelike Pairing in a New *d*<sup>9</sup> Nickelate Superconductor (Nd,Sr)NiO<sub>2</sub>, *Phys. Rev. Lett.* **125**, 077003 (2020).
  - [23] B. Kang, C. Melnick, P. Semon, S. Ryee, M. J. Han, G. Kotliar, and S. Choi, Infinite-layer nickelates as Ni-*e<sub>g</sub>* Hund's metals, *npj Quantum Mater.* **8**, 35 (2023).
  - [24] Y. Wang, C.-J. Kang, H. Miao, and G. Kotliar, Hund's metal physics: From SrNiO<sub>2</sub> to LaNiO<sub>2</sub>, *Phys. Rev. B* **102**, 161118 (2020).
  - [25] C.-J. Kang and G. Kotliar, Optical Properties of the Infinite-Layer La<sub>1-x</sub>Sr<sub>x</sub>NiO<sub>2</sub> and Hidden Hund's Physics, *Phys. Rev. Lett.* **126**, 127401 (2021).
  - [26] T. Y. Xie, Z. Liu, C. Cao, Z. F. Wang, J. L. Yang, and W. Zhu, Microscopic theory of superconducting phase diagram in infinite-layer nickelates, *Phys. Rev. B* **106**, 035111 (2022).